Radiation Measurements 192 (2026) 107606

Contents lists available at ScienceDirect

Radiation Measurements

journal homepage: www.elsevier.com/locate/radmeas

Swift heavy ion and UV irradiation of natural cryolite (Na_3AlF_6)

Anna Szreter [a,b,*], Adrian A. Finch [a], Henrik Friis [b], Christina Trautmann [c], Frieder Koch [c], Ina Schubert [c]

[a] School of Earth & Environmental Sciences, University of St Andrews, Bute Building, Queen's Terrace, St Andrews, KY16 9TS, UK
[b] Natural History Museum, University of Oslo, PO 1172 Blindern, 0318, Oslo, Norway
[c] GSI Helmholtzzentrum für Schwerionenforschung, Planckstr. 1, 64291, Darmstadt, Germany

ARTICLE INFO

Keywords:
Sodium hexafluoroaluminate
Swift heavy ion irradiation
Photoluminescence
Structural defects
F-centres
Ivittuut

ABSTRACT

The successful application of fluorides in dosimetry and optics has encouraged study of the optical properties of doped cryolite and cryolite-structure materials. However, natural cryolite (Na_3AlF_6) has never been described in terms of its defect structure, crucial for optical applications. To address this knowledge gap, we irradiate cryolite with ^{238}U ions and use excitation lifetime photoluminescence to constrain the defect structures formed. Untreated, high-energy ion and UV-irradiated samples are compared in terms of their emission spectra and luminescence lifetimes. Particle irradiation introduces an orange colour to originally black, purple and white cryolite. Untreated cryolite shows blue emissions at ~2.86 and ~2.60 eV (435 and 475 nm) and a green emission at 2.27 eV (545 nm). After uranium ion irradiation, the green luminescence intensity is enhanced compared to blue emissions. Subsequent ultraviolet irradiation causes ~57 % reduction in the dark blue emission intensity and 40–70 % increase in green. All luminescence lifetimes are prolonged by particle irradiation, but stay in the nanosecond range. We infer that a vacancy-related defect is produced by particle and UV irradiation and responsible for the green luminescence. Another defect, presumably electronic, is removed by particle irradiation and UV. The ~2.27 eV green luminescence centre is interpreted as an *F*-centre localised on a fluorine vacancy. The blue luminescence centres are interpreted as electron-hole pairs, localised at the AlF_6 octahedron normal lattice sites for ~2.86 eV and octahedral defect sites for ~2.60 eV. The experiment provides insight into natural defect formation processes in cryolite from the Ivittuut deposit in Southern Greenland.

1. Introduction

Several industrial applications, including dosimetry and optics, are strongly dependent on the defect structures of solids. Hence a significant body of literature has been directed to their characterisation. In recent years, industry-focused research has targeted complex halides with the cryolite (Na_3AlF_6) structure (e.g. Guo et al., 2022; Sakaguchi et al., 2023; Shuai et al., 2024). Their advantages as display materials are e.g. low-cost and high colour purity (Guo et al., 2022), while in dosimetry their effective atomic number is similar to human soft tissue (Sakaguchi et al., 2023). At present, only fluorite (CaF_2) has been characterised with sufficient detail to act as a reference for other fluorides, including aluminofluorides. Directly understanding the defect structure of cryolite would greatly enhance the further development of these materials.

Halides, and especially alkali halides, are stable, highly ionic solids with a large (6–8 eV) band gap, broadly applicable in optics. Among complex halides, the aluminofluorides are commonly described. The basic aluminofluoride is cryolite (Hawthorne and Herwig, 2021) and many other functional materials are based on its structure (e.g. K_3YF_6 - Shuai et al., 2020; Cs_3CeI_6 - Guo et al., 2022; $(NH_4)_3FeF_6$ - Sun et al., 2013). The cryolite structure is a double perovskite structure. It contains isolated AlF_6 octahedra, linked to two crystallographically different Na atoms, one occupying a regular octahedron (sixfold coordinated) and the other a distorted cubic antiprism (eightfold coordinated). The structure is monoclinic at room temperature, but due to small distortion from 90° it appears pseudocubic (Hawthorne and Ferguson, 1975). Low-temperature cryolite that has been through the cubic-monoclinic transition is characterised by polysynthetic twinning. Aluminium substitutions for Na (Al_{Na}) are reported (Foy and Madden, 2006) and other defect structures are expected. Jansen et al. (2023) determined the band gap for cryolite as ~7 eV whereas for the related mineral chiolite ($Na_5Al_3F_{14}$), it was found to be 5.94 eV (Wang et al., 2022).

* Corresponding author. School of Earth & Environmental Sciences, University of St Andrews, Bute Building, Queen's Terrace, St Andrews, KY16 9TS, UK.
E-mail addresses: iguania@op.pl (A. Szreter), aaf1@st-andrews.ac.uk (A.A. Finch), henrik.friis@nhm.uio.no (H. Friis), C.Trautmann@gsi.de (C. Trautmann), Fr.Koch@gsi.de (F. Koch), i.schubert@gsi.de (I. Schubert).

https://doi.org/10.1016/j.radmeas.2026.107606
Received 2 September 2025; Received in revised form 19 November 2025; Accepted 6 January 2026
Available online 9 January 2026

Particle irradiation induces new defect structures in solids, which can then be correlated with spectroscopic properties. Such experiments have been successfully used to understand defect structures in simple halides (e.g. Aguilar et al., 1979; Bangert et al., 1982; Abu-Hassen and Townsend, 1986; Trautmann et al., 1999). In this study, we apply uranium ion and then UV irradiation to modify the defect structure of cryolite. Swift heavy ions (SHI) are used to create substantial populations of defects, while low-energy UV irradiation is used to explore metastable defects, transient in geological time scale. This experimental setup is designed to address two major questions. First, what are the changes in cryolite after particle irradiation, recorded by photoluminescence? Second, how does subsequent exposure to UV change the photoluminescence? Finally, we compare these experimental results to the natural radiation effect on cryolite in the Ivittuut deposit in Southern Greenland, the primary location where cryolite was mined in the 19th and 20th centuries.

2. Materials and methods

In this study, natural cryolite from Ivittuut (previously spelled Ivigtût), SW Greenland, is used. To represent best the natural material, we analyse the most abundant, white variety alongside the less common purple and black cryolite variants. Two other aluminofluoride minerals from Ivittuut, cryolithionite ($Na_3Al_2(LiF_4)_3$) and chiolite ($Na_5Al_3F_{14}$), are also analysed and serve as references. All samples are cut as ~1 cm^2 irregular chips 0.5 cm thick. The original material is stored at the Natural History Museum in Oslo, Norway. Information on the investigated samples is summarized in Table 1.

Samples are irradiated at the UNILAC accelerator of the GSI Helmholtz Centre in Darmstadt (Germany) using ^{238}U ions of 1.14 GeV kinetic energy. According to the SRIM-2008 code (Ziegler et al., 2008), the depth of implantation of the U ions in cryolite is 43.9 μm. Electronic stopping dominates over nuclear stopping (99.82 % and 0.18 %, respectively). The ion flux is limited to approximately 1.5×10^8 ions/cm^2 s to avoid significant macroscopic heating of the samples. The maximum fluence applied is 10^{12} ions/cm^2 (estimated uncertainty ~10 %) corresponding to a total deposited energy of 1.54×10^7 Gy in the samples. Assuming a 5 nm track radius, at the applied fluence ~54 % of the exposed sample area is directly affected by ion tracks. The ion beam is defocussed to expose homogeneously the whole target area. During irradiation, the samples are covered with a hexagonal mesh (obscuring ~10 % of the surface) to enable a direct comparison of pristine (covered) and irradiated (exposed) materials.

Untreated and irradiated samples are examined by lifetime photoluminescence. A LifeSpec II ns-lifetime photoluminescence spectrometer (Edinburgh Instruments, housed at the University of St Andrews, UK) is used, with an EPL-375 ps pulsed diode laser (371 nm = 3.34 eV, 5 mW, pulse width 55 ps) used for sample excitation and a Hamamatsu Photosensor detector. A band-pass filter is placed behind the UV excitation source to prevent visible light contamination of the sample chamber. Similarly, a 405 nm long-pass filter is placed at the outlet of sample chamber to prevent the excitation UV radiation from reaching the detector. Data are acquired using time-correlated single photon counting.

Table 1
Sample list.

Sample	Mineral	Colour	Treatment
HF-6 w	cryolite	white	untreated
HF-5 w	cryolite	white	U-irradiated
HF-3 p	cryolite	purple	untreated
HF-1 p	cryolite	purple	U-irradiated
HF-7 b	cryolite	black	untreated & U-irradiated
Knr8422	cryolithionite	white	untreated & U-irradiated
Knr8436	chiolite	white	untreated & U-irradiated

Calibration of the spectrometer using a Hg lamp shows the accuracy of the wavelengths to be within 2 nm at the slit size used. The laser spot size is ~2 mm in diameter, but the sample is presented to the beam at an obtuse angle and hence its footprint on the sample is ~4 mm in diameter.

Experiments at a variety of repetition times (100 ns–50 μs) show that a 100 ns period provides the best constraint on the lifetimes of the active components. The lifetime data show no evidence of elevated background in the 410–650 nm range, which would point at lifetime components extending beyond the 100 ns repetition time. Two types of experiments, time-resolved emission scans (TRES) and wavelength (emission) scans, are conducted.

In a TRES scan, luminescence lifetime is first recorded for a single wavelength. The lifetime scans are obtained at 100 ns period (repetition time) for a combined integration time (dwell time) of 10 000 s. After 10 000 s, the spectrometer moves to the next wavelength with 5 nm step and the process is repeated. It takes ~1 week to complete the lifetime measurements of all wavelengths. Excitation lifetimes are fitted in Origin (2023b).

Wavelength (emission) scans are collected with the same step (5 nm) and also analysed in 410–650 nm wavelength range, but the dwell time is typically 5 s and laser repetition time is 50 ns. Emission spectra are recalculated from wavelength to photon energy (following Townsend and Rowlands, 2000) to enable deconvolution of the emission bands using multiple peak Gaussian fit in Origin. The green luminescence band usually appears under the broad envelope, while on one spectrum (UV-irradiated purple cryolite) its position clearly stands out from the envelope. Based on this spectrum, the green luminescence is fixed at 2.27 eV to increase the fit confidence.

The step-by-step measurement procedure is as follows:

1. Wavelength scan of untreated samples (measurement time is ~5 min). Results are recalculated from nanometres to electron volts and through deconvolution, wavelengths of particular luminescence centres are determined.
2. TRES scan of untreated samples. At the wavelengths of identified luminescence centres, decay plots are extracted. Decay times (lifetimes) are fitted in Origin.
3. Samples are irradiated by SHI ex-situ (outside the photoluminescence spectrometer).
4. Wavelength scan of SHI irradiated samples.
5. TRES scan of SHI irradiated samples. During the scan, the UV laser irradiates the sample surface for 7 days and 7 h.
6. Wavelength scan of UV-exposed SHI-irradiated samples.

Note that UV exposure occurs *in situ* (inside the luminescence spectrometer), while SHI irradiation happens *ex situ* (samples are removed from the spectrometer). The luminescence intensity is not directly comparable when a sample is removed from the instrument and then replaced.

3. Results

3.1. Colour change

After uranium ion irradiation, the honeycomb pattern of the mesh used to cover the samples becomes visible on all cryolite samples. The irradiated areas become orange-brownish while the protected areas keep their original colour (Fig. 1). Unlike cryolite, the irradiated cryolithionite and chiolite samples retain their original colour (Fig. 1). The irradiation indicates that a small orange area in the cryolithionite chip (Knr8422) is cryolite. Similarly, an area of HF-1p that remains uncoloured during ion irradiation consists of another aluminofluoride mineral.

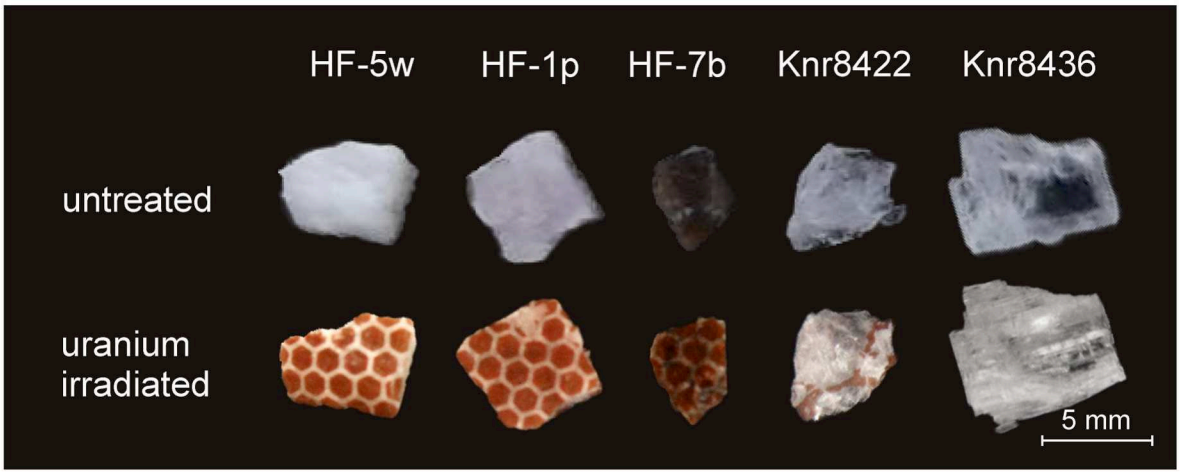

Fig. 1. Colouration effect induced by the irradiation with 1.14 GeV U ions. The honeycomb pattern results from a mesh placed in front of the samples to separate irradiated and non-irradiated areas.

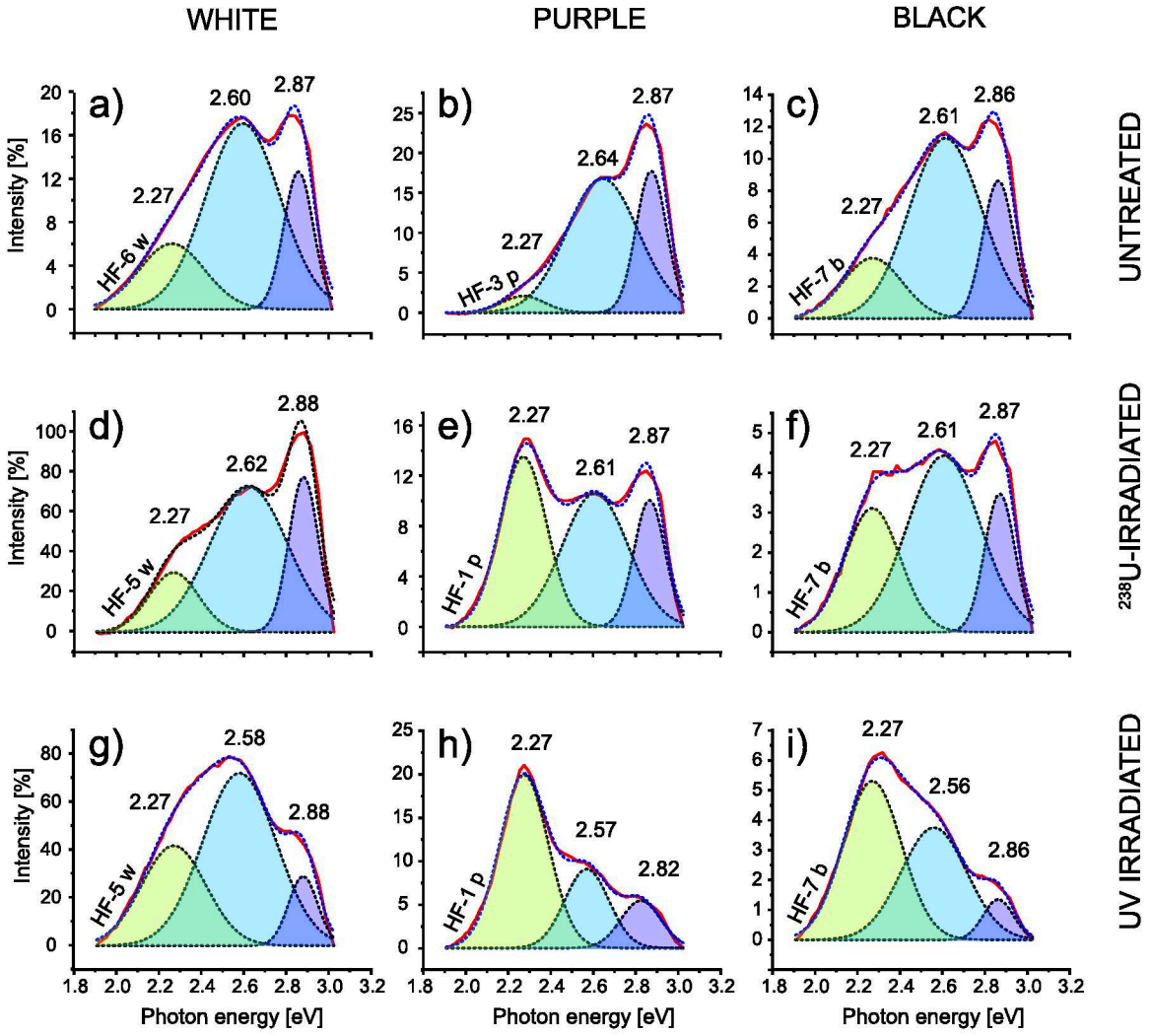

Fig. 2. Emission spectra of white, purple and black cryolite; untreated (top row), irradiated with 10^{12} U-ions/cm^2 (central row) and exposed to UV (bottom row). The wavelength (emission) scans data are converted into phonon energy (solid red line) and deconvoluted to reveal single emissions (dashed line). Note that SHI irradiation was done ex situ (the samples were removed from the spectrometer after scans a-c were obtained), while UV irradiation was done *in situ* (without moving the samples). Removing and re-mounting of a sample chip with irregular surface means that intensities are directly comparable between d-f and g-i but not between a-c and the other scans. Wavelength scan parameters: 3.34 eV excitation energy, 55 ps pulse width, 5 s dwell time, 50 ns laser repetition time, room temperature. (For interpretation of the references to colour in this figure legend, the reader is referred to the Web version of this article.)

3.2. Ion irradiation influence on luminescence spectra

The emission spectra of cryolite are presented in Fig. 2 and details are given in Table 2. Cryolite has three luminescence bands: green at 2.27 eV (fixed in our fitting), pale blue at ~2.60 and dark blue at ~2.86 (typical 2σ precisions 0.02 and 0.01 eV, respectively). In untreated white and black cryolite, the dark blue luminescence has twice, and the pale blue almost three times the intensity of the green luminescence (Fig. 2a–c). In purple cryolite, the difference between green and blue luminescence intensity is eightfold (Fig. 2b).

The absolute luminescence intensities before and after SHI irradiation are not directly comparable (see Methods section for more details), but the relative intensities can be broadly compared. Upon ion irradiation, the relative intensities of the pale and dark blue luminescence bands are retained in coloured cryolites and slightly changed in white (Fig. 2d–f). In white cryolite, the green luminescence is also retained (Fig. 2d), while in coloured cryolites its relative intensity increases to approach (black cryolite) or overtake (purple cryolite) the dark blue luminescence (Fig. 2e and f).

3.3. UV exposure influence on luminescence spectra

Exposure to UV during the TRES scans further modifies the emission spectra of the SHI irradiated samples (Fig. 2g–i). The green luminescence further increases by 40, 48 and 71 % in white, purple and black cryolite, respectively. The pale blue luminescence intensity is constant in white cryolite and drops by 15 % in both purple and black cryolite. Significant changes are observed in dark blue luminescence, which decreases in intensity by 46 % (purple cryolite) and ~60 % (white and black cryolite). Macroscopically, in all cryolite samples, the area illuminated by the UV laser loses the orange colour from ion irradiation and turns white (Fig. 3).

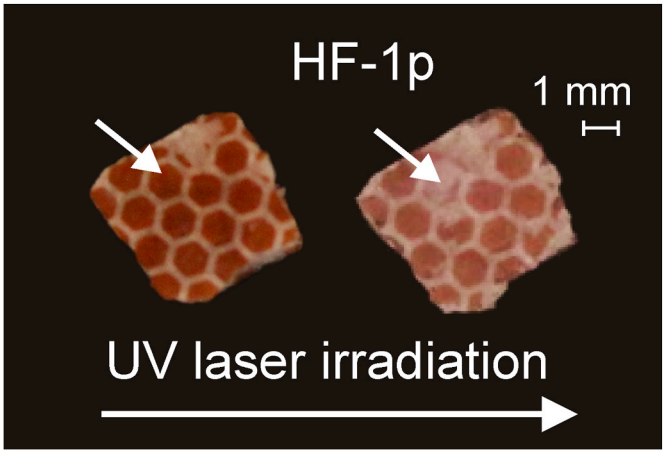

Fig. 3. Purple cryolite sample irradiated with U ions before (left) and after (right) UV bleaching (3.34 eV, 7 days, room temperature). The arrows mark the beam spot of the UV laser.

3.4. Ion irradiation influence on luminescence lifetimes

Luminescence lifetimes are calculated from the TRES scans and hence represent samples (untreated and SHI irradiated) partially

Table 2
Deconvoluted spectra details. The spectra result from wavelength (emission) scans and fitting in Origin using Gaussian fit. Wavelength scan parameters: 3.34 eV excitation energy, 55 ps pulse width, 5 s dwell time, 50 ns laser repetition time, room temperature.

Colour	Sample	Impl.	UV	Lum.	PP	2σ	FWHM	2σ	Height	2σ	x^2_{red}	R^2	Fig. 2.
White	HF-6 w	no	no	green	2.27	*n.a.*	0.36	*0.03*	6.01	*0.98*	0.246	0.995	a)
				pale blue	2.60	*0.01*	0.41	*0.05*	17.04	*0.48*			
				dark blue	2.87	*0.00*	0.16	*0.02*	12.62	*1.91*			
	HF-5 w	yes	no	green	2.27	*n.a.*	0.28	*0.03*	29.78	*6.68*	12.623	0.989	d)
				pale blue	2.62	*0.03*	0.43	*0.08*	72.71	*2.99*			
				dark blue	2.88	*0.01*	0.16	*0.03*	77.53	*14.67*			
	HF-5 w	yes	yes	green	2.27	*n.a.*	0.36	*0.01*	41.69	*3.33*	2.328	0.997	g)
				pale blue	2.58	*0.01*	0.41	*0.03*	71.99	*1.57*			
				dark blue	2.88	*0.01*	0.16	*0.02*	28.85	*3.87*			
Purple	HF-3 p	no	no	green	2.27	*n.a.*	0.24	*0.09*	2.07	*0.90*	0.472	0.993	b)
				pale blue	2.64	*0.03*	0.40	*0.06*	16.75	*0.70*			
				dark blue	2.87	*0.01*	0.17	*0.02*	17.71	*3.33*			
	HF-1 p	yes	no	green	2.27	*0.01*	0.26	*0.02*	13.46	*1.40*	0.159	0.994	e)
				pale blue	2.61	*0.02*	0.36	*0.11*	10.60	*0.35*			
				dark blue	2.87	*0.01*	0.17	*0.02*	10.03	*2.34*			
	HF-1 p	yes	yes	green	2.27	*0.01*	0.27	*0.01*	19.86	*0.49*	0.201	0.996	h)
				pale blue	2.57	*0.02*	0.24	*0.06*	9.04	*0.66*			
				dark blue	2.82	*0.03*	0.22	*0.06*	5.43	*0.88*			
Black	HF-7 b	no	no	green	2.27	*n.a.*	0.33	*0.03*	3.78	*0.65*	0.139	0.994	c)
				pale blue	2.61	*0.02*	0.40	*0.06*	11.28	*0.35*			
				dark blue	2.86	*0.01*	0.17	*0.02*	8.62	*1.70*			
	HF-7 b	yes	no	green	2.27	*n.a.*	0.30	*0.02*	3.10	*0.28*	0.025	0.993	f)
				pale blue	2.61	*0.02*	0.40	*0.06*	4.42	*0.14*			
				dark blue	2.87	*0.01*	0.17	*0.02*	3.46	*0.59*			
	HF-7 b	yes	yes	green	2.27	*n.a.*	0.32	*0.01*	5.29	*0.19*	0.011	0.998	i)
				pale blue	2.56	*0.01*	0.36	*0.03*	3.74	*0.11*			
				dark blue	2.86	*0.01*	0.17	*0.03*	1.35	*0.20*			

2σ – precision of the preceding value, ^{238}U – irradiation with 1.14 GeV uranium ions, UV – exposure to ultraviolet (372 nm, typically 7 days), Lum. – luminescence, PP - peak position [eV], FWHM - full width at half maximum [eV], Height – peak intensity [% of the highest measured, not fitted, intensity], x^2_{red} - reduced chi-square, R^2 - coefficient of determination, n.a. – not applicable (fixed peak position).
Note that apart from the fit error (2σ), the instrumental error (2.5 nm) should be taken into account when comparing the data. The 2.5 nm error equals to 0.01 eV in the green and pale blue luminescence regions and 0.02 eV in the dark blue luminescence region.

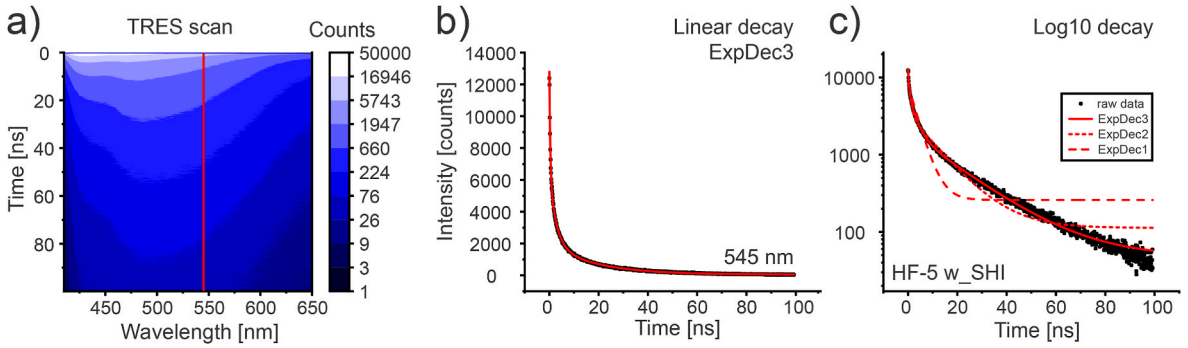

Fig. 4. Lifetime measurement procedure, exemplified on SHI-irradiated HF-5w. (a) A selected wavelength (in this case 545 nm = 2.27 eV), marked by the red line, is extracted from a TRES scan (this is done on raw data and only demonstrated on the plot for clarity). (b) Decay plot at 545 nm with linear scale on y axis. The red line represents exponential decay function fitted to 3 components. (c) Decay plot at 545 nm with logarithmic scale on y axis. This plot demonstrates how exponential decays fitted to one or two components (dashed red lines) are insufficient to represent the data, while fitting to three components (solid red line) represents them more significantly. (For interpretation of the references to colour in this figure legend, the reader is referred to the Web version of this article.)

Table 3
Luminescence excitation lifetimes, extracted from TRES scans and fitted in Origin using Gaussian fit. TRES scan parameters: 3.34 eV excitation energy, 55 ps pulse width, 10 000 s dwell time, 100 ns laser repetition time, room temperature.

Sample	Band	R^2	A_0	2σ	τ_0	2σ	A_1	2σ	τ_1	2σ	A_2	2σ	τ_2	2σ
HF-6 w untreated	2.27	0.998	571	*15*	**0.21**	*0.01*	866	*12*	**1.24**	*0.03*	277	*8*	**6.17**	*0.12*
	2.60	0.999	761	*32*	**0.18**	*0.01*	4211	*27*	**1.02**	*0.01*	779	*15*	**5.46**	*0.07*
	2.86	1.000	1349	*56*	**0.20**	*0.01*	8716	*48*	**0.92**	*0.01*	878	*22*	**4.77**	*0.08*
HF-5 w ion irradiated	2.27	0.999	6282.53	*117*	**0.38**	*0.01*	4541	*95*	**2.70**	*0.09*	1923	*49*	**18.69**	*0.51*
	2.60	0.999	9825	*185*	**0.35**	*0.01*	11857	*154*	**2.21**	*0.04*	3845	*78*	**14.04**	*0.25*
	2.86	0.999	22646	*722*	**0.52**	*0.02*	15252	*598*	**2.29**	*0.12*	3593	*301*	**11.29**	*0.66*
HF-1 p untreated	2.27	0.999	3290	*52*	**0.21**	*<0.01*	4057	*41*	**1.13**	*0.02*	2134	*45*	**4.31**	*0.05*
	2.60	0.999	6125	*84*	**0.24**	*<0.01*	5477	*73*	**1.13**	*0.02*	1104	*32*	**6.14**	*0.12*
	2.86	1.000	9099	*73*	**0.19**	*<0.01*	9521	*62*	**1.00**	*0.01*	1467	*31*	**5.30**	*0.08*
HF-1 p ion irradiated	2.27	0.999	14728	*214*	**0.34**	*0.01*	17463	*168*	**2.60**	*0.05*	2438	*161*	**12.66**	*0.62*
	2.60	0.999	10240	*160*	**0.34**	*0.01*	9215	*134*	**2.03**	*0.04*	2187	*65*	**12.57**	*0.32*
	2.86	0.999	13423	*209*	**0.29**	*0.01*	11697	*168*	**1.63**	*0.04*	2334	*105*	**8.36**	*0.27*
HF-7 b untreated	2.27	0.991	162.51	*6*	**0.15**	*0.01*	145	*5*	**1.17**	*0.07*	88	*5*	**5.00**	*0.18*
	2.60	0.996	287	*22*	**0.28**	*0.02*	415	*21*	**0.96**	*0.04*	72	*4*	**5.48**	*0.22*
	2.86	0.998	1381	*124*	**0.42**	*0.02*	739	*121*	**0.97**	*0.08*	53	*9*	**5.55**	*0.59*
HF-7 b ion irradiated	2.27	0.999	5887.32	*64*	**0.25**	*0.01*	4575	*47*	**2.43**	*0.05*	833	*36*	**14.92**	*0.59*
	2.60	0.999	15504	*273*	**0.34**	*0.01*	9861	*247*	**1.60**	*0.05*	1086	*70*	**10.96**	*0.61*
	2.86	0.999	20237	*397*	**0.28**	*0.01*	9645	*363*	**1.17**	*0.04*	798	*87*	**7.88**	*0.69*

Band – band position [eV], R^2 – fit control parameter, A_0, A_1, A_2 – intensity [counts]; τ_0, τ_1, τ_2 – lifetime [ns], 2σ – precision of the preceding value. τ_0 have values characteristic of the excitation laser afterpulse and thus are not interpreted as lifetime components. The intensity data are collected under similar conditions using the same instrument and are therefore considered broadly comparable.

modified by UV exposure (Fig. 4, Table 3). Exponential decay models with one, two and three variables are tested, and three variables model best represents the data (i.e. optimising the F-value statistical parameter) (Fig. 4c). Our fitting indicates lifetime components in all samples of ~0.3 ns but we are cautious in interpreting these values since the laser has a small afterpulse typically 0.2–0.3 ns after the main pulse. We are therefore unconfident to attribute these very fast (<0.5 ns) decays to a genuine response of the sample. These very fast pulses are reported in Table 3 as τ_0 but not interpreted.

The fit is optimised with a short (0.92–2.70 ns, τ_1) and a longer (4.31–18.69 ns, τ_2) lifetime component for all the samples (Table 3). Before irradiation, no major differences in luminescence lifetimes are observed between particular bands, as well as between cryolite varieties.

Ion irradiation causes all lifetimes to increase (Table 3). For green luminescence the lifetime component τ_1 doubles and τ_2 triples. Blue luminescence lifetimes show more increase in white cryolite (~120–160 %) and less in coloured cryolite (~20–100 %). The ~2.86 eV luminescence lifetime is most dependent on the cryolite colour, increasing by ca. 20–40 % in black, 60 % in purple and 140–150 % in white cryolite.

4. Discussion

The experiment is designed to compare and contrast the response of cryolite to highly ionizing particle irradiation and lower energy UV exposure.

The data indicate that four major changes occur in cryolite on irradiation with U ions: (1) the irradiated sample layer becomes orange. (2) The relative intensity of green luminescence at ~2.27 eV increases in coloured cryolite, but remains unaffected in white cryolite. (3) After the subsequent UV exposure, the intensity of the dark blue emission at ~2.86 eV is halved, followed by minor decrease of the pale blue emission at ~2.60 eV and 40–71 % increase of the green emission intensities. (4) All luminescence lifetimes increase after ion irradiation, but remain in nanosecond range. Altogether, these results suggest that green luminescence centres (presumably vacancy-related defect) are introduced in significant amounts by SHI and UV irradiation. At the same time, blue luminescence centres (presumably electronic defects) are diminished under both SHI irradiation and UV exposure. These changes are further discussed in the following sections.

4.1. Colour change

As a result of swift heavy ion irradiation cryolite is coloured orange. Particle irradiation introduces structural defects, modifying the colour and/or luminescence properties of a material. A "yellow to dark brown" colouration of alkali halides on Bi irradiation was reported in LiF (Trautmann et al., 1999; Sorokin et al., 2014) and MgF_2 (El-Said et al., 2006) and this is reminiscent of the colour change seen here. In LiF and MgF_2, this change was ascribed to *F* and F_2 colour centres (i.e. an electron trapped in a vacancy, or two such defects next to each other).

4.2. Luminescence band positions

In one spectrum (Fig. 2h), the green luminescence is clear and we therefore use this spectrum to identify the peak position (2.27 eV, 545 nm). This constraint improves the robustness of the fitting of the other spectra where the peak lies under a broad envelope, and is difficult to deconvolute. Apparent minor differences in the blue luminescence bands can be observed in Fig. 2. However, these differences are within the fitting precision (2σ in Table 2) and instrumental accuracy (2.5 nm at 5 nm spacing of data acquisition). Therefore, we see no strong evidence for the peak position shifts and focus on the statistically significant changes in intensity. Consequently, we have chosen an average emission energy to represent the blue emissions in cryolite: dark blue at ~2.86 eV (435 nm) and pale blue at ~2.60 eV (475 nm).

4.3. Swift heavy ion irradiation

Uranium ion irradiation enhances the green luminescence (~2.27 eV) intensity, relative to blue luminescence intensities (~2.60 and ~2.85 eV). The change is strong in coloured cryolite but weak in white cryolite. The absolute values indicate a drop in dark blue luminescence intensity in the coloured cryolites (Fig. 2e and f), but an approximately sixfold increase in the white cryolite (Fig. 2d). As mentioned above, the absolute values of Fig. 2a-c and Fig. 2d-f are not directly comparable due to sample removal and repositioning in the spectrometer. Therefore, we focus on the relative changes at this step.

Changes in the intensity ratio between two luminescence bands have been observed in other particle irradiation experiments. This usually took the form of a decrease in intensity of one luminescence centre and an increase in another. For instance, a shift from orange to blue luminescence in quartz was attributed to crystal amorphization (Townsend, 1987). However, SHI-irradiated fluorides remain crystalline due to strong ionic binding (Trautmann et al., 2000; El-Said et al., 2002; Schwartz et al., 2003). King et al. (2011) explained a shift from UV-violet to red luminescence on He irradiation in quartz as redistribution of electrons between different luminescence centres. Electron transfer between two luminescence centres may also be a process relevant for cryolite and aligns with the absolute intensity changes between Fig. 2b–c and e–f. While the current data cannot confirm this mechanism unambiguously, it offers a reasonable and internally consistent explanation.

4.4. UV-irradiation

The extended exposure of our samples to ultraviolet (3.3 eV, 372 nm, typically 7 days) results in a 46–60 % decrease in the dark blue emission intensity and only a minor reduction in the pale blue emission, together with a 40–71 % intensity increase in the green emission. The green emission intensity increase is lower in white and purple cryolite than in black cryolite (Table 2, Fig. 2d–j). This demonstrates the high stability of the ~2.60 eV centre to UV exposure and the more effective removal of the ~2.86 eV centre.

The energy of the UV used (3.3–eV) is too low to directly displace ions from their lattice sites. However, UV photons can create electronic excitations as well as self-trapped excitons which can decay into a Frenkel defect. Also, UV exposure can induce bleaching of colour centres, a well-known phenomenon in ionic crystals, semiconductors, and insulators (e.g. Lecoq et al., 2017). Excitation of electrons trapped in colour centres or other defect states can lead to recombination with nearby vacancies deleting or transforming the original colour centres. *F*-centres and their aggregates are known to be produced by particle irradiation (e.g. Trautmann et al., 1999; Alghamdi and Townsend, 1990; Townsend and Wang, 2024) and UV (e.g. Friis et al., 2007; Townsend and Wang, 2024).

In our samples, the observed shift in ~2.86 eV dark blue luminescence after UV exposure is likely due to the conversion of one type luminescence centre into another, possibly into the ~2.27 eV green emission centre. The results presented here do not allow for unambiguous identification of the exact nature of the defect centres. However, the decay of electron-hole type defects, and subsequent formation and recharging of vacancy type defects, reasonably explains the luminescence transitions we observe.

4.5. Luminescence centres

All observed luminescence lifetimes fall within the nanosecond range (0.92–18.33–ns, Table 3). This rules out the possibility that the luminescence originates from intra-ion energy cascades in transition metals or lanthanides, which have much longer (e.g. μs) lifetimes, indicating that the signal is dominated by structural defects (e.g. Caldwell, 2021; Cheng, 2023). In materials where luminescence is solely related to structural defects, variation in the nanosecond lifetimes can reflect the physical dispersion of the defect centres. Faster luminescence and energy quenching are characteristic of defect clusters (Zhou, 2018). In this study, all lifetimes increase after ion irradiation, which can be interpreted as dispersion of clustered defects, as was recorded in $LiNbO_3$, another perovskite-based structure (Haycock and Townsend, 1987). More precisely, irregular cluster sizes in ion irradiated material compared to untreated material result in broader emission peaks and longer lifetimes. Defect de-clustering restricts energy quenching (Sundara Rao et al., 2013), but enhances the quantum efficiency of luminescence (Kalpana et al., 2016; Horsburgh et al., 2023). This is consistent with the overall luminescence intensity increase after ion irradiation (A_1 and A_2 values in Table 3). Thus, we infer that the luminescence centres discussed in the following paragraphs are clustered in the natural material, even though the exact nature and number of neighbouring centres are not accessible from our data.

4.5.1. Blue luminescence (2.86 & 2.60 eV, 435 & 475 nm)

All cryolite samples show a narrow (FWHM ~0.17 eV), dark blue emission at ~2.86 eV (435 nm) and a broad (FWHM ~0.4 eV), pale blue emission at ~2.60 eV (475 nm). We are not aware of any description of these luminescence bands in cryolite. Emissions at 430 and 470 nm in a cryolite-structure Cs_3CeI_6 were ascribed to lanthanide ions (Guo et al., 2022). However, the broad bands with nanosecond lifetimes are inconsistent with lanthanides, which produce sharp bands with milli- to microsecond lifetimes (Caldwell, 2021). Emissions at 440 and 475 nm were also observed in $LiNbO_3$ (Haycock and Townsend, 1987). $LiNbO_3$ containing NbO_6 octahedra ionically bonded to Li may serve as an analogue for cryolite, which contains AlF_6 octahedra ionically bonded to Na. The two materials have different band gaps, but defect-related electronic processes associated with similar octahedral units can provide useful insights into the defect structure of cryolite. $LiNbO_3$ luminescence at 400–500 nm is related to a Nb^{4+}_{Nb} - O^- polaron, i.e. hole and electron pairs, recombining on the octahedral cluster (Kämpfe et al., 2016; Smirnov et al., 2023). In this material, exciton polarons bound to Li vacancies (v_{Li}) are generally more stable than polarons at lattice positions (Schmidt et al., 2022). Luminescence from electron-hole recombination on tetrahedral sites at ~400 nm was also observed in leucophanite ($NaCaBeSi_2O_6F$) (Friis et al., 2007). Finally, recombination of electrons with self-trapped holes was interpreted as an intrinsic

feature, producing blue luminescence in AgCl (Grigorjeva et al., 1995). Another type of electron-hole pairs, exciton-like formations, produce 400 and 443 nm luminescence in KCl:Na (Shunkeyev et al., 2025).

Based on these closest analogues available, the blue luminescence in cryolite is concluded to result from electron-hole recombination. The exact nature of these pairs (electron-hole pair, exciton, bound exciton, exciton polaron etc.) cannot yet be precisely determined. By analogy with $LiNbO_3$, we hypothesise these features are related to the AlF_6 octahedron in cryolite. To test this, we analyse UV photoluminescence from natural cryolithionite ($Na_3Al_2(LiF_4)_3$) (Fig. 5a) and chiolite ($Na_5Al_3F_{14}$) (Fig. 5b), aluminofluorides which also have AlF_6 octahedra in their structures. Similar emission bands are observed, which is consistent with the recombination centres being associated with the AlF_6 entity. This could be e.g. an Al^{2+}_{Al}-F^- pair, or AlF^+_5-F^- octahedron with dominance of the ionic bond in one Al-F pair. Finally, the higher stability of the ~2.60 eV pale blue luminescence can reflect electron-hole recombination on a vacancy in the AlF_6 octahedron (Schmidt et al., 2022). The less stable dark blue luminescence is more likely localised on a regular octahedral site (Table 4, Fig. 6).

4.5.2. Green luminescence (2.27 eV, 545 nm)

Green luminescence at ~2.27 eV is enhanced in cryolite by uranium ion irradiation and its intensity is further amplified by subsequent UV exposure. We are not aware of any previous description of luminescence at this energy caused by structural defects in natural or synthetic cryolite. A 550 nm emission was reported in Tb-doped cryolite and ascribed to Tb (Sakaguchi et al., 2023), while Cr- and Mn-doped cryolite do not show luminescence in this region (Zhou, 2018; Hong et al., 2019). In NaCl, a 517 nm (2.4 eV) emission was ascribed to F_2-centres (Aguilar et al., 1979), while 518 and 540 nm absorptions in LiF were interpreted as F_4-centres, i.e. four clustered F-centres (Trautmann et al., 1999). However, luminescence in the 500–600 nm region was ascribed to point defects in $LiNbO_3$, including Nb_{Li} substitutions (520 nm; Krol et al., 1980), V_{Li} vacancies (532 nm) and Nb_{Nb}-Nb_{Li} bipolarons (540 nm) (Smirnov et al., 2023).

The swift heavy ion irradiation of cryolite is expected to produce Frenkel defects (i.e. vacancies and interstitial pairs) in both Na and F. In cryolite, Al_{Na} substitutions have been reported (Foy and Madden, 2006), and polaron formation on them is a feasible mechanism. Vacancies are also well-established intrinsic defects in halides (e.g. Lidiard, 1962), from which F-centres are produced by irradiation (e.g. Trautmann et al., 1999; Luschik et al., 2018). Decay of such a pair will release energy, which could immediately excite another electron and lead to its entrapment in neighbouring V_F vacancy to create an F-centre (Table 4, Fig. 6).

4.6. Relation to natural systems

Natural cryolite contains radioactive elements (such as U and Th) which decay via multiple alpha emissions. Over geological time scales (e.g. 1.27 Ga at Ivittuut – Köhler et al., 2008), exposure to alpha particles (~4.4 MeV for ^{235}U, 4.0 MeV for ^{232}Th) produces a similar damage as the irradiation performed in this study using the uranium beam. The penetration depth is three times smaller (13.8 μm for He, 43.9 μm for U), but in both cases electronic stopping largely dominates over nuclear stopping. The average energy deposition along the trajectory of 1.14 GeV U ions is approximately 26 keV/nm and is 87 times larger than for 4 MeV alpha particles (0.3 keV/nm). Hence the energy deposited through U irradiation per unit volume in this experiment is of the same order of magnitude as the energy deposited by natural decay processes in the Ivittuut deposit for 1.27 billion years. The specific doses are comparable: 10^{12} U/ions/cm^2 correspond to 1.54×10^7 Gy and 1.27 Ga corresponds to 9.77×10^6 Gy, respectively. However, when comparing the effects caution is needed, as at the high energy densities of uranium ions, the formation of cluster defects becomes pronounced. Compared to simple defects induced by alpha particles, defect clusters can modify the luminescence properties in slightly different ways.

The two blue luminescence centres enhanced by ion irradiation are present in natural cryolite. However, the much greater age of geological timescales potentially allows natural samples to adopt more optimised defect clustering. Moreover, thermally induced diffusion, although slow, would in longer timeframes reverse the formation of many Frenkel defects. The ion irradiation therefore, although providing insights in the processes, does not create materials that are exact analogues of minerals.

5. Conclusions

In this study, we investigate how the luminescence behaviour of cryolite changes when irradiated with high-energy ^{238}U ions. Lifetime photoluminescence is used to characterise the defect centres and their behaviour both directly after ion irradiation and following UV exposure. Untreated cryolite has three luminescence centres: green at ~2.27 eV pale blue at ~2.60 eV and dark blue at ~2.86 eV. The irradiation with 10^{12} cm^{-2} U ions enhances the green luminescence and extinguishes the blue luminescence, though the latter can be an actual effect or an artefact of sample re-positioning. The changes in intensity of the blue and green luminescence may be interconnected. Exposure of the ion-irradiated samples to UV causes orange colour bleaching and a significant decrease of the ~2.86 eV emission, a minor decrease of the ~2.60 eV and a simultaneous increase of the ~2.27 eV emission. One possible explanation of this behaviour is that the blue luminescence originates from electron-hole type defects, and the green luminescence relates to vacancies. The decay of blue luminescence centres by UV exposure

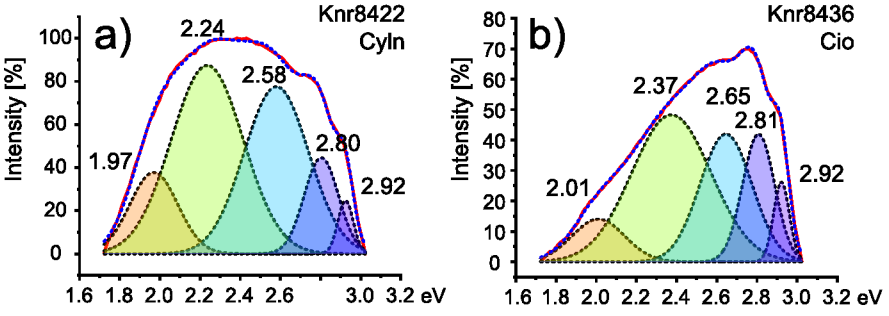

Fig. 5. Deconvolution of (a) cryolithionite and (b) chiolite luminescence. Red solid line shows the experimental data, dashed lines show the fitted peaks and their envelope. Note that the peak at 2.92 eV represents a tail of a peak >3 eV, cut off by the filter. Wavelength scan parameters: 3.34 eV excitation energy, 55 ps pulse width, 5 s dwell time, 50 ns laser repetition time, room temperature. (For interpretation of the references to colour in this figure legend, the reader is referred to the Web version of this article.)

Table 4
Summary and interpretation of luminescence centres in cryolite.

Energy [eV]	Wavelength [nm]	Luminescence	Ion irradiation	UV irradiation	Centre type	Location
2.86	435	dark blue	significant increase	significant decrease	e^{-}-h^{+} pair	defect-free octahedral site
2.60	475	pale blue	increase	minor decrease	e^{-}-h^{+} pair	octahedral vacancy
2.27	545	green	introduced	increase	*F*-centre	fluorine vacancy

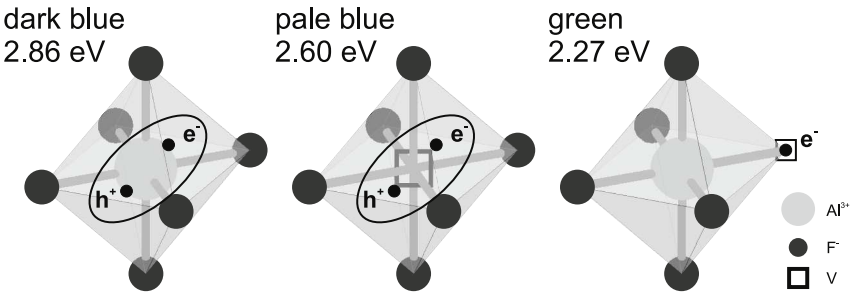

Fig. 6. Proposed assignments of luminescence centres in cryolite. Blue luminescence is interpreted as electron-hole pair type defect on the AlF_6 octahedron. More stable pale blue luminescence can be localised on a vacancy, while less stable dark blue luminescence on a regular structural position. Green luminescence is interpreted as *F*-centre in the place of fluorine vacancy.

allows the released energy to directly enhance the green luminescence. Luminescence lifetimes in the nanosecond range are inconsistent with transition metal impurities but consistent with structural defects. The increase of luminescence lifetime on uranium irradiation could be due to dispersion in size of defect clusters. Both blue (~2.60 and ~2.86 eV) luminescence centres are attributed to electron-hole type defect recombination on the AlF_6 octahedron. Due to its higher stability under UV exposure, the ~2.60 eV pale blue luminescence centre may be bound to a vacancy on the octahedron, which is unaffected during irradiation. The ~2.27 eV green luminescence is interpreted as *F*-centres formed at fluorine vacancies. Uranium irradiation of cryolite modifies the material through similar mechanisms as α-particle irradiation over geological timescales (1.27 Ga). Therefore, this study offers insight into processes by which defects form in natural cryolite such as found in the Ivittuut deposit.

CRediT authorship contribution statement

Anna Szreter: Writing – review & editing, Writing – original draft, Visualization, Investigation, Formal analysis. **Adrian A. Finch:** Writing – review & editing, Supervision, Project administration, Methodology, Investigation, Funding acquisition, Conceptualization. **Henrik Friis:** Writing – review & editing, Supervision, Resources, Funding acquisition, Conceptualization. **Christina Trautmann:** Writing – review & editing, Methodology, Conceptualization. **Frieder Koch:** Writing – review & editing, Investigation. **Ina Schubert:** Writing – review & editing, Investigation.

Declaration of competing interest

The authors declare that they have no known competing financial interests or personal relationships that could have appeared to influence the work reported in this paper.

Acknowledgements

This project was funded as a co-tutelle studentship by the Global Doctoral Scholarship from the University of St Andrews and Natural History Museum in Oslo. The fieldwork was kindly supported by Eclipse Metals Ltd and the assistance of Carl Popal is greatly appreciated. Many thanks for assistance during fieldwork to: Curtis Rooks, Ninni Jeremiassen, Thomas Ulrich and the *Sanatit* crew. The results presented here are based on a UMAT experiment, which was performed at the M-branch of the UNILAC at the GSI Helmholtzzentrum für Schwerionenforschung, Darmstadt (Germany) in the frame of FAIR Phase-0.

Appendix A. Supplementary data

Supplementary data to this article can be found online at https://doi.org/10.1016/j.radmeas.2026.107606.

Data availability

Data will be made available on request.

References

Abu-Hassen, L.H., Townsend, P.D., 1986. Ion implantation in LiF to form F and F_2 centres. J. Phys. C Solid State Phys. 19 (2), 99. https://doi.org/10.1088/0022-3719/19/2/007.

Aguilar, M., Chandler, P.J., Townsends, P.D., 1979. Luminescence of NaCl—I. Electron and ion beam excited spectra. Radiat. Eff. 40 (1–2), 1–7. https://doi.org/10.1080/00337577908234484.

Alghamdi, A., Townsend, P.D., 1990. Luminescence efficiency during ion implantation of sapphire. Radiat. Eff. Defect Solid 115 (1–3), 73–78. https://doi.org/10.1080/10420159008220555.

Bangert, U., Thiel, K., Ahmed, K., Townsend, P.D., 1982. I-The emission spectra of tl produced by ion implanted CaF_2. Radiat. Eff. 64 (1–4), 143–151. https://doi.org/10.1080/00337578208223005.

Caldwell, J., 2021. Geological Histories Encoded in Fast Fluorescence Lifetimes of Fluorite. University of St Andrews, UK. MSc thesis.

Cheng, P., 2023. Lanthanides: Fundamentals and Applications. Elsevier, Amsterdam.

El-Said, A.S., Neumann, R., Schwartz, K., Trautmann, C., 2002. Heavy ion induced damage in MgF_2 crystals. Radiat. Eff. Defect Solid 157 (6–12), 649–654. https://doi.org/10.1080/10420150215795.

El-Said, A.S., Neumann, R., Schwartz, K., Trautmann, C., 2006. Swelling and creation of color centers in MgF_2 single crystals irradiated with energetic heavy ions. Nucl. Instrum. Methods Phys. Res. Sect. B Beam Interact. Mater. Atoms 245 (1), 250–254. https://doi.org/10.1016/j.nimb.2005.11.110.

Foy, L., Madden, P.A., 2006. Ionic motion in crystalline cryolite. J. Phys. Chem. B 110 (31), 15302–15311. https://doi.org/10.1021/jp062563o.

Friis, H., Finch, A.A., Townsend, P.D., Hole, D.E., El Mkami, H., 2007. Ionoluminescence of leucophanite. Am. Mineral. 92 (2–3), 254–260. https://doi.org/10.2138/am.2007.2167.

Grigorjeva, L.G., Kotomin, E.A., Millers, D.K., Eglitis, R.I., 1995. The decay kinetics of excitonic luminescence in AgCl crystals. J. Phys. Condens. Matter 7 (7), 1483. https://doi.org/10.1088/0953-8984/7/7/027.

Guo, Q., Wang, L., Yang, L., Duan, J., Du, H., Ji, G., Liu, N., Zhao, X., Chen, C., Xu, L., Gao, L., Luo, J., Tang, J., 2022. Spectra stable deep-blue light-emitting diodes based on cryolite-like cerium (III) halides with nanosecond d-f emission. Sci. Adv. 8 (50). https://doi.org/10.1126/sciadv.abq2148 eabq2148.

Hawthorne, F.C., Ferguson, R.B., 1975. Refinement of the crystal structure of cryolite. Can. Mineral. 13 (4), 377–382.

Hawthorne, F.C., Herwig, S., 2021. A structure hierarchy for the aluminofluoride minerals. Can. Mineral. 59 (1), 211–241. https://doi.org/10.3749/canmin.2000047.

Haycock, P.W., Townsend, P.D., 1987. Exciton luminescence from pure $LiNbO_3$. J. Phys. C Solid State Phys. 20 (2), 319. https://doi.org/10.1088/0022-3719/20/2/014.

Hong, F., Xu, H., Yang, L., Liu, G., Song, C., Dong, X., Yu, W., 2019. Mn^{4+} nonequivalent-doped Al^{3+}-based cryolite high-performance warm WLED red phosphors. New J. Chem. 43, 14859–14871. https://doi.org/10.1039/C9NJ03607E.

Horsburgh, N.J., Finch, A.A., Friis, H., 2023. Lanthanide and yttrium substitution in natural fluorite. Phys. Chem. Miner. 50 (2), 15. https://doi.org/10.1007/s00269-023-01239-4.

Jansen, T., Böhnisch, D., Baur, F., Jüstel, T., 2023. On the optical properties of monoclinic Na_3AlF_6 and Na_3AlF_6: Mn^{4+}. Opt. Mater. X 20, 100276. https://doi.org/10.1016/j.omx.2023.100276.

Kalpana, T., Gandhi, Y., Sudarsan, V., Piasecki, M., Ravi Kumar, V., Veeraiah, N., 2016. Improving green emission of Tb^{3+} ions in $BaO\text{-}B_2O_3\text{-}P_2O_5$ glasses by means of Al^{3+} ions. Luminescence 31 (7), 1358–1363. https://doi.org/10.1002/bio.3115.

Kämpfe, T., Haußmann, A., Eng, L.M., Reichenbach, P., Thiessen, A., Woike, T., Steudtner, R., 2016. Time-resolved photoluminescence spectroscopy of NbNb4+and O^- polarons in $LiNbO_3$ single crystals. Phys. Rev. B 93 (17), 174116. https://doi.org/10.1103/PhysRevB.93.174116.

King, G.E., Finch, A.A., Robinson, R.A.J., Hole, D.E., 2011. The problem of dating quartz 1: spectroscopic ionoluminescence of dose dependence. Radiat. Meas. 46 (1), 1–9. https://doi.org/10.1016/j.radmeas.2010.07.031.

Krol, D.M., Blasse, G., Powell, R.C., 1980. The influence of the Li/Nb ratio on the luminescence properties of $LiNbO_3$. J. Chem. Phys. 73 (1), 163–166. https://doi.org/10.1063/1.439901.

Köhler, J., Konnerup-Madsen, J., Markl, G., 2008. Fluid geochemistry in the Ivigtut cryolite deposit, South Greenland. Lithos 103 (3–4), 369–392. https://doi.org/10.1016/j.lithos.2007.10.005.

Lecoq, P., Gektin, A., Korzhik, M., Lecoq, P., Gektin, A., Korzhik, M., 2017. Influence of crystal structure defects on scintillation properties. In: Lecoq, P., et al. (Eds.), Inorganic Scintillators for Detector Systems: Physical Principles and Crystal Engineering, pp. 197–252.

Lidiard, A.B., 1962. Reactions among point defects in alkali halides. J. Appl. Phys. 33 (1), 414–421. https://doi.org/10.1063/1.1777133.

Lushchik, A., Lushchik, C., Vasil'Chenko, E., Popov, A.I., 2018. Radiation creation of cation defects in alkali halide crystals: review and today's concept. Low Temp. Phys. 44 (4), 269–277. https://doi.org/10.1063/1.5030448.

Sakaguchi, H., Fukushima, H., Kato, T., Nakauchi, D., Kawaguchi, N., Yanagida, T., 2023. Photoluminescence and dosimetric properties of Tb-doped Na_3AlF_6 ceramics. J. Lumin. 254, 119533. https://doi.org/10.1016/j.jlumin.2022.119533.

Schmidt, F., Kozub, A.L., Gerstmann, U., Schmidt, W.G., Schindlmayr, A., 2022. A density-functional theory study of hole and defect-bound exciton polarons in lithium niobate. Crystals 12 (11), 1586. https://doi.org/10.3390/cryst12111586.

Schwartz, K., Trautmann, C., Neumann, R., 2003. Electronic excitations and heavy-ion-induced processes in ionic crystals. Nucl. Instrum. Methods Phys. Res. Sect. B Beam Interact. Mater. Atoms 209, 73–84. https://doi.org/10.1016/S0168-583X(02)02013-X.

Shuai, P., Yang, D., Liao, L., Guo, Q., Mei, L., Zhang, Y., Liu, H., 2020. Preparation, structure and up-conversion luminescence properties of novel cryolite K_3YF_6: Er^{3+}, Yb^{3+}. RSC Adv. 10 (3), 1658–1665. https://doi.org/10.1039/C9RA10257D.

Shuai, P., Guo, Q., Liao, L., Su, K., Ding, J., An, N., Mei, L., Woźny, P., Runowski, M., 2024. Preparation and sensing performance study in ultra-wide temperature range of K3LuF6: Er3+, Yb3+ up-converting luminescent materials with cryolite structure. Ceram. Int. 50 (17), 30879–30886. https://doi.org/10.1016/j.ceramint.2024.05.393.

Shunkeyev, K., Kenzhebayeva, A., Krasnikov, A., Nagirnyi, V., Sagimbayeva, S., Sergeyev, D., Tilep, A., Ubaev, Z., Lushchik, A., 2025. Luminescence of bound excitons created near sodium impurity ions in KCl: na single crystals. Opt. Mater. X 25, 100395. https://doi.org/10.1016/j.omx.2024.100395.

Smirnov, M.V., Sidorov, N.V., Palatnikov, M.N., 2023. Luminescence properties of non-stoichiometric lithium niobate crystals of various composition and genesis. Opt Spectrosc. 131 (8), 743–756. https://doi.org/10.1134/S0030400X23060164.

Sorokin, M.V., Schwartz, K., Trautmann, C., Dauletbekova, A., El-Said, A.S., 2014. Modeling of defect accumulation in lithium fluoride crystals under irradiation with swift ions. Nucl. Instrum. Methods Phys. Res. Sect. B Beam Interact. Mater. Atoms 326, 307–310. https://doi.org/10.1016/j.nimb.2013.10.033.

Sun, J., Qiu, T., Wang, J., Liu, H., Yang, W., 2013. Phase-transfer-based synthesis of $(NH_4)_3FeF_6$ and its application as an anode material for lithium-ion batteries. Mater. Lett. 93, 39–41. https://doi.org/10.1016/j.matlet.2012.11.021.

Sundara Rao, M., Sudarsan, V., Brik, M.G., Bhargavi, K., Rao, C.S., Gandhi, Y., Veeraiah, N., 2013. The de-clustering influence of aluminum ions on the emission features of Nd^{3+} ions in $PbO\text{–}SiO_2$ glasses. Opt. Commun. 298, 135–140. https://doi.org/10.1016/j.optcom.2013.02.011.

Townsend, P.D., 1987. Optical effects of ion implantation. Rep. Prog. Phys. 50 (5), 501. https://doi.org/10.1088/0034-4885/50/5/001.

Townsend, P.D., Rowlands, A.P., 2000. Information encoded in cathodoluminescence emission spectra. In: Cathodoluminescence in Geosciences. Springer Berlin Heidelberg, Berlin, Heidelberg, pp. 41–57.

Townsend, P.D., Wang, Y., 2024. Improving interpretations of imperfections in insulating materials for current technologies. Opt. Mater. X, 100327. https://doi.org/10.1016/j.omx.2024.100327.

Trautmann, C., Schwartz, K., Steckenreiter, T., 1999. Specificity of ion induced damage. Nucl. Instrum. Methods Phys. Res. Sect. B Beam Interact. Mater. Atoms 156 (1–4), 162–169. https://doi.org/10.1016/S0168-583X(99)00247-5.

Trautmann, C., Toulemonde, M., Schwartz, K., Costantini, J.M., Müller, A., 2000. Damage structure in the ionic crystal LiF irradiated with swift heavy ions. Nucl. Instrum. Methods Phys. Res. Sect. B Beam Interact. Mater. Atoms 164, 365–376. https://doi.org/10.1016/S0168-583X(99)01066-6.

Wang, D., Lv, P., Fang, L., Zhou, X., Zhang, J., Xia, H., Song, H., Chen, B., 2022. Growth of $KAlF_4$ and $Na_5Al_3F_{14}$ aluminum fluoride single crystals by Bridgman method. Cryst. Res. Technol. 57 (6), 2200013. https://doi.org/10.1002/crat.202200013.

Zhou, Y., 2018. Optical Functionalization of Cryolite Polycrystals Using Transition metal/rare Earth Ions for the Applications of Lighting and Biological Imaging. The State University of New Jersey, USA, Rutgers. MSc thesis.

Ziegler, J.F., Ziegler, M.D., Biersack, J.P., 2008. SRIM-2008-04. Maryland, Freeware, Annapolis. http://www.srim.org.